Journal of Systems Engineering and Electronics
Vol. 35, No. 3, June 2024, pp.589 – 598

# Beamspace maximum likelihood algorithm based on sum and difference beams for elevation estimation

CHEN Sheng, ZHAO Yongbo*, HU Yili, and PANG Xiaojiao

National Laboratory of Radar Signal Processing, Xidian University, Xi'an 710071, China

**Abstract:** Beamspace super-resolution methods for elevation estimation in multipath environment has attracted significant attention, especially the beamspace maximum likelihood (BML) algorithm. However, the difference beam is rarely used in super-resolution methods, especially in low elevation estimation. The target airspace information in the difference beam is different from the target airspace information in the sum beam. And the use of difference beams does not significantly increase the complexity of the system and algorithms. Thus, this paper applies the difference beam to the beamformer to improve the elevation estimation performance of BML algorithm. And the direction and number of beams can be adjusted according to the actual needs. The theoretical target elevation angle root means square error (RMSE) and the computational complexity of the proposed algorithms are analyzed. Finally, computer simulations and real data processing results demonstrate the effectiveness of the proposed algorithms.

**Keywords:** elevation estimation, beamspace, multipath environment, maximum likelihood.

**DOI:** 10.23919/JSEE.2024.000057

## 1. Introduction

In recent decades, target height estimation in multipath environment has attracted significant attention [1–3]. The target height is directly calculated by the elevation angle, so the height estimation is equivalent to the elevation angle estimation. The direct signal and reflected signals passing along the Earth's surface enter the radar's main beam together. The direct and reflected signals are indistinguishable in time, Doppler, and space domain, resulting in a degradation of target elevation estimation performance [4,5]. The reflected signals are not limited to only one path, but are equivalent to one path by the echo with a broad spatial extent in the Fresnel reflection area [6,7]. Thus, this paper assumes that the reflected signals only contain the specular reflection signal. Additionally, array radar may not handle data from massive arrays very well in element-space because of the large data transmission, storage, and computation [8]. Therefore, many beamspace algorithms convert the data from element-space to a lower-dimensional beamspace and then estimate target angle [9–11]. Compared with the processing in element-space, the processing in beamspace can obtain better performance by losing certain degrees of freedom, such as lower signal to noise ratio (SNR) resolution threshold, reduced amount of data transmission, storage, and computation [10,11].

The angle estimation algorithms based on sum and difference beams are classical methods in monopulse radar [12–14]. However, for monopulse methods, the reflected signal can only be regarded as interference and is eliminated in multipath environment [15] in general, and the information about the space domain in the reflected signal is lost. Although the monopulse methods based on sum and difference beams are also used in array radar [16,17], the estimation performance is still limited due to the low degree of freedom of the beam. The discrete Fourier transform (DFT) matrix is good beamformer for beamspace methods, which can obtain good angle estimation performance [10]. Additionally, super-resolution methods, i.e., the methods that break through the Rayleigh resolution limit [18], such as subspace algorithms and maximum likelihood (ML) schemes, are currently the main elevation estimation methods in element-space. Therefore, the beamspace super-resolution methods using DFT matrix beamformer are good candidates for elevation estimation.

The subspace algorithms, such as multiple signal classification (MUSIC) [19] and estimating signal parmeters via rotationsl invariance techniques (ESPRIT) [20], usually require more snapshots and losing a certain aperture to realize signal decoherent processing [21]. In [22], the covariance matrix in beamspace was reconstructed into the covariance matrix in element-space, and then the

Manuscript received July 07, 2022.
*Corresponding author.
This work was supported by the Fund for Foreign Scholars in University Research and Teaching Programs (B18039).

angles of coherent signals are estimated using spatial smoothing MUSIC algorithm in element-space. In [23], the beamspace U-ESPRIT algorithm performs two dimensional (2D) estimation of azimuth angle and elevation angle for coherently sources in multiple input multiple output (MIMO) radar. The beamspace unitary-ESPRIT (U-ESPRIT) algorithm choose proper and few beams in 2D-beamspace to reduce computational complexity. ML algorithm [24] can directly process coherent signals and can operate utilizing a single snapshot. The refined ML (RML) algorithm [3,25] in element-space makes full use of the prior knowledge of geometric information and surface reflection coefficient and uses a composite guide vector, i.e., the refined signal model, instead of a conventional guide vector. Thus, the RML algorithm has high estimation accuracy and low computational burden, but is sensitive to parameter errors due to the refined signal model mismatch [26]. The three dimensional (3D) beamspace ML (BML) algorithm [2] offers a closed-form solution for elevation estimation by the feature that the eigenvector of the beamspace correlation matrix associated with the smallest eigenvalue is orthogonal to the subspace spanned by the signals, so it has very low computational complexity. In addition, [2] also developed the 2D BML algorithm, which offers a closed-form solution without considering multipath. The 2D-BML algorithm is suitable for the initial estimation of tracking or the scenes without multipath. On the basis of the 3D-BML algorithm, the multipath scenario with interference or an extra target was discussed [27]. In [28], the BML algorithm for elevation estimation in MIMO radar was proposed to reduce the computational burden. In [29], the angle estimation for transmit beamspace-based in bistatic MIMO radar was developed. The authors design the transmit beamspace through convex optimization to focus the transmitted energy. However, this method is not suitable for conventional phased array radar.

To the best of our knowledge, the beamspace super-resolution methods for elevation estimation in multipath environment have not been found to consider the difference beam yet. In order to improve the accuracy of BML algorithm for elevation estimation, this paper applies the difference beam to the beamformer and discuss two settings of sum and difference beams that can meet the needs of most elevation estimation scenarios. The concept of sum and difference beams adopted in this paper is more extensive than that of the traditional sum and difference beams. The traditional sum and difference beams is generally a pair of sum and difference beams, which is a special case of the sum and difference beams in this paper. The number of sum and difference beams and the beam direction in this paper can be flexibly set. Then, a beamspace ML algorithm based on sum and difference beams (ML-SDB) is proposed. The ML-SDB algorithm does not need the surface reflection parameters, i.e., it is not affected by the corresponding errors. Taking the refined signal model [3,25] into account in the ML-SDB algorithm, a beamspace refined ML-SDB (RML-SDB) is developed. Our simulation results show that compared with the ML-SDB algorithm, the RML-SDB algorithm has higher estimation accuracy and lower computational burden, although it is sensitive to antenna height and reflection coefficient errors.

This paper is structured as follows. Section 2 provides a multipath signal model. Section 3 reviews the 3D-BML algorithm briefly, proposes the ML-SDB and RML-SDB algorithms for elevation estimation, and gives the theoretical elevation angle root mean square error (RMSE). Section 4 analyses the computational complexity of the proposed algorithms. Finally, Section 5 evaluates the proposed algorithms in various simulations and real data processing results, while Section 6 concludes this work.

## 2. Multipath signal model

Consider a digital array radar equipped with a uniform linear array. The geometry for a smooth earth model with multipath propagation is presented in Fig. 1. The linear array with the $M$ elements receives the two paths of target echoes from the different directions of arrival. One path returns directly from the target to the radar antenna, whereas another path returns from the reflecting surface, where the incident angle of the direct and reflected signals are $\theta_1$ and $\theta_2$, respectively. The height of the array radar centre is $h_r$. The distance between two adjacent array elements is $d$, which is half the wavelength. The height of the target is $h_t$. The distance from the target to the array radar centre is $R_d$.

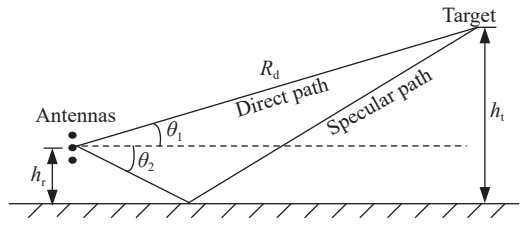


**Fig. 1 Multipath geometry model of low-angle target**

For the array radar system, the received signal in element-space can be written as

$$\boldsymbol{x}(l)=[\boldsymbol{a}(\theta_1),\boldsymbol{a}(\theta_2)]\begin{bmatrix}\alpha(l)\\ \alpha(l)\rho\mathrm{e}^{-\mathrm{j}\varphi(\theta_1)}\end{bmatrix}+\boldsymbol{n}(l)=\boldsymbol{A}\boldsymbol{c}(l)+\boldsymbol{n}(l),\ l=1,2,\cdots,L \tag{1}$$

where $L$ is the number of snapshots, and $\boldsymbol{a}(\theta)\in\mathbf{C}^{M\times 1}$ is

called the array steering vector defined as

$$\boldsymbol{a}(\theta)=\left[\mathrm{e}^{-\mathrm{j}\pi d(M-1)\sin\theta/\lambda},\mathrm{e}^{-\mathrm{j}\pi d(M-3)\sin\theta/\lambda},\cdots,\mathrm{e}^{\mathrm{j}\pi d(M-1)\sin\theta/\lambda}\right]^{\mathrm{T}} \quad (2)$$

where $\lambda$ is the working wavelength, $d=\lambda/2$, $\alpha(l)$ the complex amplitude related to target characteristics at the $l$th snapshot, and $\rho$ the surface reflection coefficient. The surface reflection coefficient $\rho$ is generally expressed as $\rho=\Gamma D\rho_s$, where $\Gamma$ denotes the smooth surface reflection coefficient, $D$ the divergence factor and $\rho_s$ the surface roughness factor [25], but it can be regarded as a constant for the scenario in this paper [30]. $\varphi(\theta_1)\approx 4\pi h_r\sin\theta_1/\lambda$ is the phase-difference between the direct and reflected signals due to time delay. $\boldsymbol{n}(l)\in\mathbf{C}^{M\times 1}$ is the Gaussian white noise vector with zero mean at the $l$th snapshot, which is not correlated with the target signals. The variance matrix of $\boldsymbol{n}(l)$ is $\sigma_n^2\boldsymbol{I}_M$. $\boldsymbol{I}_M$ represents an identity matrix of size $M\times M$.

Consider a unitary matrix beamformer, as

$$\boldsymbol{T}=\frac{1}{\sqrt{M}}\left[\boldsymbol{a}\left(\theta^1\right),\boldsymbol{a}\left(\theta^2\right),\cdots,\boldsymbol{a}\left(\theta^Q\right)\right] \quad (3)$$

where $\boldsymbol{T}\in\mathbf{C}^{M\times Q}$, $\boldsymbol{T}^{\mathrm{H}}\boldsymbol{T}=\boldsymbol{I}_Q$, and $Q$ is the number of beams, which is different when used in different methods. Then, using $\boldsymbol{T}$ to convert $\boldsymbol{x}(l)$ from element-space to beamspace, the received data in beamspace is formed as

$$\boldsymbol{x}_B(l)=\boldsymbol{T}^{\mathrm{H}}\boldsymbol{x}(l)=\boldsymbol{T}^{\mathrm{H}}\boldsymbol{A}\boldsymbol{c}(l)+\boldsymbol{T}^{\mathrm{H}}\boldsymbol{n}(l)=\boldsymbol{B}\boldsymbol{c}(l)+\boldsymbol{n}_B(l) \quad (4)$$

where $\boldsymbol{B}=\boldsymbol{T}^{\mathrm{H}}\boldsymbol{A}$ and $\boldsymbol{n}_B(l)=\boldsymbol{T}^{\mathrm{H}}\boldsymbol{n}(l)$ is still Gaussian white noise vector.

## 3. Beamspace ML algorithm based on sum and difference beams

This section reviews the 3D-BML algorithm briefly, and presents the proposed ML-SDB and RML-SDB algorithms for elevation estimation.

### 3.1 Previous 3D-BML algorithm

The 3D-BML algorithm [2] considers a $M\times 3$ unitary matrix beamformer

$$\boldsymbol{T}_{3D}=\frac{1}{\sqrt{M}}\left[\boldsymbol{a}\left(-\frac{2}{M}\right),\ \boldsymbol{a}(0),\ \boldsymbol{a}\left(\frac{2}{M}\right)\right] \quad (5)$$

including a reference beam pointing 0, and two auxiliary beams pointing to $-2/M$ and $2/M$. Then, the 3D-BML estimations of $\theta_1$ and $\theta_2$ are the solution to the following optimization problem:

$$\underset{\theta_1,\theta_2,\boldsymbol{c}(1),\boldsymbol{c}(2),\cdots,\boldsymbol{c}(L)}{\text{Minimize}}\ \sum_{l=1}^{L}\|\boldsymbol{x}_B(l)-\boldsymbol{B}\boldsymbol{c}(l)\|_2^2 \quad (6)$$

where $\|\cdot\|_2$ denotes the 2-norm, $\boldsymbol{B}=\boldsymbol{T}_{3D}^{\mathrm{H}}\boldsymbol{A}$. Utilize the separability to obtain the respective least square error solution $\boldsymbol{c}_{\mathrm{LS}}(l)=[\boldsymbol{B}^{\mathrm{H}}\boldsymbol{B}]^{-1}\boldsymbol{B}^{\mathrm{H}}\boldsymbol{x}_B(l)$ $(l=1,2,\cdots,L)$. Substitute $\boldsymbol{c}_{\mathrm{LS}}(l)$ for $\boldsymbol{c}(l)$ in (6), we get

$$\underset{\theta_1,\theta_2}{\text{Minimize}}\ \sum_{l=1}^{L}\boldsymbol{x}_{\boldsymbol{B}}^{\mathrm{H}}(l)\,\boldsymbol{P}_{\boldsymbol{B}}^{\perp}(\theta_1,\theta_2)\,\boldsymbol{x}_{\boldsymbol{B}}(l) \quad (7)$$

where $\boldsymbol{P}_B^{\perp}(\theta_1,\theta_2)=\boldsymbol{I}_3-\boldsymbol{B}[\boldsymbol{B}^{\mathrm{T}}\boldsymbol{B}]^{-1}\boldsymbol{B}^{\mathrm{T}}$. The solution of (7) is given in [2].

### 3.2 ML-SDB algorithm

Without loss of generality, suppose the number of array elements is even, and $M=2K$, where $K$ is an integer. We define matrices as follows:

$$\boldsymbol{T}_1=\frac{1}{\sqrt{M}}\left[\boldsymbol{a}_1\left(\theta^1\right),\boldsymbol{a}_1\left(\theta^2\right),\cdots,\boldsymbol{a}_1\left(\theta^Q\right)\right], \quad (8)$$

$$\boldsymbol{T}_2=\frac{1}{\sqrt{M}}\left[\boldsymbol{a}_2\left(\theta^1\right),\boldsymbol{a}_2\left(\theta^2\right),\cdots,\boldsymbol{a}_2\left(\theta^Q\right)\right], \quad (9)$$

where

$$\begin{cases}\boldsymbol{a}_1(\theta^q)=\left[\mathrm{e}^{-\mathrm{j}\pi d(M-1)\sin\theta^q/\lambda},\mathrm{e}^{-\mathrm{j}\pi d(M-3)\sin\theta^q/\lambda},\cdots,\mathrm{e}^{-\mathrm{j}\pi d\sin\theta^q/\lambda}\right]^{\mathrm{T}}\\ \boldsymbol{a}_2(\theta^q)=\left[\mathrm{e}^{\mathrm{j}\pi d\sin\theta^q/\lambda},\mathrm{e}^{\mathrm{j}3\pi d\sin\theta^q/\lambda},\cdots,\mathrm{e}^{\mathrm{j}\pi d(M-1)\sin\theta^q/\lambda}\right]^{\mathrm{T}}\end{cases}. \quad (10)$$

It can be seen that $\boldsymbol{T}=[\boldsymbol{T}_1,\ \boldsymbol{T}_2]^{\mathrm{T}}$, $\boldsymbol{T}_1,\boldsymbol{T}_2\in\mathbf{C}^{K\times Q}$, and $\boldsymbol{a}_2(\theta^q)=\boldsymbol{a}_1(\theta^q)\mathrm{e}^{\mathrm{j}\pi dM\sin\theta^q/\lambda}$. Then, the received data in beamspace can be rewritten as

$$\boldsymbol{x}_{\mathrm{B}}(l)=\boldsymbol{T}^{\mathrm{H}}\boldsymbol{x}(l)=\boldsymbol{T}_1^{\mathrm{H}}\boldsymbol{x}_1(l)+\boldsymbol{T}_2^{\mathrm{H}}\boldsymbol{x}_2(l)=\boldsymbol{x}_{\mathrm{Bs}}(l) \quad (11)$$

where $\boldsymbol{x}(l)=[\boldsymbol{x}_1(l),\ \boldsymbol{x}_2(l)]^{\mathrm{T}}$ and $\boldsymbol{x}_1(l),\boldsymbol{x}_2(l)\in\mathbf{C}^{K\times 1}$. It can be seen from (11) that the array is divided into two equal subarrays, and $\boldsymbol{x}_{\mathrm{Bs}}$ is the sum of the subarrays in beamspace. We can easily get the difference of the subarrays in beamspace, as

$$\boldsymbol{x}_{\mathrm{Bd}}(l)=\boldsymbol{T}_1^{\mathrm{H}}\boldsymbol{x}_1(l)-\boldsymbol{T}_2^{\mathrm{H}}\boldsymbol{x}_2(l). \quad (12)$$

Then, we get the sum and difference data in beamspace

$$\boldsymbol{x}_{\boldsymbol{B}\mathrm{sd}}(l)=\begin{bmatrix}\boldsymbol{x}_{\mathrm{Bs}}(l)\\ \boldsymbol{x}_{\mathrm{Bd}}(l)\end{bmatrix}=\begin{bmatrix}\boldsymbol{T}_1^{\mathrm{H}}\boldsymbol{x}_1(l)+\boldsymbol{T}_2^{\mathrm{H}}\boldsymbol{x}_2(l)\\ \boldsymbol{T}_1^{\mathrm{H}}\boldsymbol{x}_1(l)-\boldsymbol{T}_2^{\mathrm{H}}\boldsymbol{x}_2(l)\end{bmatrix}=\begin{bmatrix}\boldsymbol{T}_1 & \boldsymbol{T}_1\\ \boldsymbol{T}_2 & -\boldsymbol{T}_2\end{bmatrix}^{\mathrm{H}}\begin{bmatrix}\boldsymbol{x}_1(l)\\ \boldsymbol{x}_2(l)\end{bmatrix} \quad (13)$$

Define the sum and difference matrix beamformer as follows:

$$\boldsymbol{T}_{\mathrm{sd}}=\begin{bmatrix}\boldsymbol{T}_1 & \boldsymbol{T}_1\\ \boldsymbol{T}_2 & -\boldsymbol{T}_2\end{bmatrix}. \quad (14)$$

The left half of $\boldsymbol{T}_{\mathrm{sd}}$ represents sum beamformer, and the right half represents difference beamformer.

In what follows, we demonstrate the advantage of $\boldsymbol{T}_{\mathrm{sd}}$ over the $\boldsymbol{T}_{3\mathrm{D}}$ by array patterns. Consider the linear array with the 30 elements, $d=\lambda/2$, the beams in $\boldsymbol{T}_{3\mathrm{D}}$ pointing to $-2/M$, 0, and $2/M$, and the beams in $\boldsymbol{T}_{\mathrm{sd}}$ pointing to $-2/M$ and $2/M$. The array patterns of $\boldsymbol{T}_{3\mathrm{D}}$ and $\boldsymbol{T}_{\mathrm{sd}}$ are depicted in Fig. 2 and Fig. 3, respectively. It is shown that

$\boldsymbol{T}_{\rm sd}$ with only two directions has wider spatial coverage and higher effective gain than $\boldsymbol{T}_{\rm 3D}$ with three directions. The wider spatial coverage means that the elevation range occupied by the main lobe of the beamformer is larger, and the higher effective gain means that the beamformer has higher gain at a certain elevation. Wider spatial coverage and higher effective gain can make the target have higher SNR in beamspace, thus improving the estimation accuracy of the proposed methods. In addition, the beam settings can be adjusted according to actual needs. For example, for the case where the spatial range of interest is large, select the beams pointing to $-4/M$, 0, and $4/M$ to construct the sum and difference matrix beamformer. The corresponding array patterns are depicted in Fig. 4. This figure shows that the spatial coverage is wider than the coverage in Fig. 3. The two beam pointing conditions of $\boldsymbol{T}_{\rm sd}$ in Fig. 3 and Fig. 4 meet the needs of most low elevation estimation scenarios, where the elevation range is below 12°, because when target elevation is higher, the surface reflection coefficient becomes so small that the reflected signal does not need to be considered [5].

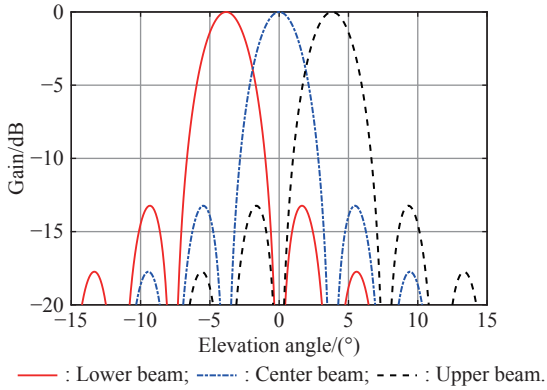


**Fig. 2 Array patterns for $\boldsymbol{T}_{\rm 3D}$ with the beams pointing to $-2/M$, 0, and $2/M$**

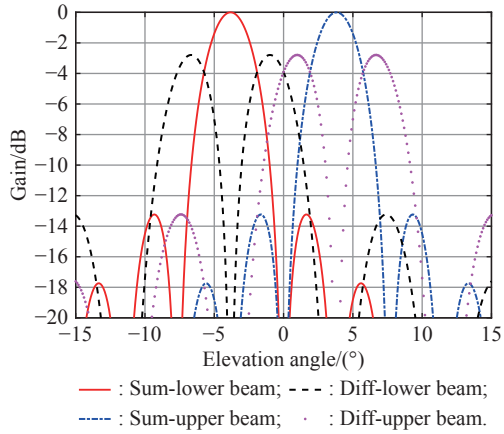


**Fig. 3 Array patterns for $\boldsymbol{T}_{\rm sd}$ with the beams pointing to $-2/M$ and $2/M$**

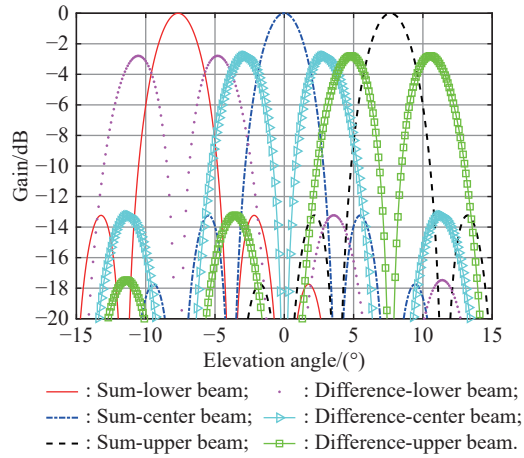


**Fig. 4 Array patterns for $\boldsymbol{T}_{\rm sd}$ with the beams pointing to $-4/M$, 0, and $4/M$.**

In addition, any method of generating difference beams can be used to obtain the sum and difference matrix beamformer. Further, the sum and difference data in beamspace can be rewritten as

$$\boldsymbol{x}_{\rm Bsd}(l)=\boldsymbol{T}_{\rm sd}^{\rm H}\boldsymbol{x}(l)=\boldsymbol{T}_{\rm sd}^{\rm H}\boldsymbol{A}\boldsymbol{c}(l)+\boldsymbol{T}_{\rm sd}^{\rm H}\boldsymbol{n}(l)=\boldsymbol{B}_{\rm sd}\boldsymbol{c}(l)+\boldsymbol{n}_{\rm Bsd}(l) \tag{15}$$

where $\boldsymbol{B}_{\rm sd}=\boldsymbol{T}_{\rm sd}^{\rm H}\boldsymbol{A}$ and $\boldsymbol{n}_{\rm Bsd}(l)=\boldsymbol{T}_{\rm sd}^{\rm H}\boldsymbol{n}(l)$. Next, in order to make better use of ML algorithm, we analyze the properties of $\boldsymbol{T}_{\rm sd}$. Because $\boldsymbol{T}$ is a unitary matrix, we have $\boldsymbol{T}^{\rm H}\boldsymbol{T}=\boldsymbol{T}_1^{\rm H}\boldsymbol{T}_1+\boldsymbol{T}_2^{\rm H}\boldsymbol{T}_2=\boldsymbol{I}_Q$. From (14), we have

$$\boldsymbol{T}_{\rm sd}^{\rm H}\boldsymbol{T}_{\rm sd}=\begin{bmatrix}\boldsymbol{T}_1^{\rm H}\boldsymbol{T}_1+\boldsymbol{T}_2^{\rm H}\boldsymbol{T}_2 & \boldsymbol{T}_1^{\rm H}\boldsymbol{T}_1-\boldsymbol{T}_2^{\rm H}\boldsymbol{T}_2\\ \boldsymbol{T}_1^{\rm H}\boldsymbol{T}_1-\boldsymbol{T}_2^{\rm H}\boldsymbol{T}_2 & \boldsymbol{T}_1^{\rm H}\boldsymbol{T}_1+\boldsymbol{T}_2^{\rm H}\boldsymbol{T}_2\end{bmatrix}=\begin{bmatrix}\boldsymbol{I}_Q & \boldsymbol{T}_1^{\rm H}\boldsymbol{T}_1-\boldsymbol{T}_2^{\rm H}\boldsymbol{T}_2\\ \boldsymbol{T}_1^{\rm H}\boldsymbol{T}_1-\boldsymbol{T}_2^{\rm H}\boldsymbol{T}_2 & \boldsymbol{I}_Q\end{bmatrix} \tag{16}$$

where

$$\boldsymbol{T}_1^{\rm H}\boldsymbol{T}_1=\frac{1}{M}\begin{bmatrix}\boldsymbol{a}_1^{\rm H}(\theta^1)\boldsymbol{a}_1(\theta^1) & \boldsymbol{a}_1^{\rm H}(\theta^1)\boldsymbol{a}_1(\theta^2) & \cdots & \boldsymbol{a}_1^{\rm H}(\theta^1)\boldsymbol{a}_1(\theta^Q)\\ \boldsymbol{a}_1^{\rm H}(\theta^2)\boldsymbol{a}_1(\theta^1) & \boldsymbol{a}_1^{\rm H}(\theta^2)\boldsymbol{a}_1(\theta^2) & \cdots & \boldsymbol{a}_1^{\rm H}(\theta^2)\boldsymbol{a}_1(\theta^Q)\\ \vdots & \vdots & \ddots & \vdots\\ \boldsymbol{a}_1^{\rm H}(\theta^Q)\boldsymbol{a}_1(\theta^1) & \boldsymbol{a}_1^{\rm H}(\theta^Q)\boldsymbol{a}_1(\theta^2) & \cdots & \boldsymbol{a}_1^{\rm H}(\theta^Q)\boldsymbol{a}_1(\theta^Q)\end{bmatrix}. \tag{17}$$

The element at the $u$ row and $v$ column of $\boldsymbol{T}_2^{\rm H}\boldsymbol{T}_2$ is

$$\left(\boldsymbol{T}_2^{\rm H}\boldsymbol{T}_2\right)_{uv}=\frac{1}{M}\boldsymbol{a}_2^{\rm H}(\theta^u)\boldsymbol{a}_2(\theta^v)=\frac{1}{M}\boldsymbol{a}_1^{\rm H}(\theta^u){\rm e}^{-\frac{{\rm j}\pi dM\sin\theta^u}{\lambda}}\boldsymbol{a}_1(\theta^v){\rm e}^{\frac{{\rm j}\pi dM\sin\theta^v}{\lambda}}=\left(\boldsymbol{T}_1^{\rm H}\boldsymbol{T}_1\right)_{uv}(\boldsymbol{F})_{uv}, \tag{18}$$

$$(\boldsymbol{F})_{uv}=\exp({\rm j}\pi dM(\sin\theta^v-\sin\theta^u)/\lambda). \tag{19}$$

For the case with the beams pointing to $-2/M$ and $2/M$, we have

$$\boldsymbol{F}=\begin{bmatrix}1 & \mathrm{e}^{\mathrm{j}\pi dM\left(\sin\theta^2-\sin\theta^1\right)/\lambda}\\ \mathrm{e}^{\mathrm{j}\pi dM\left(\sin\theta^1-\sin\theta^2\right)/\lambda} & 1\end{bmatrix}=\begin{bmatrix}1 & 0\\ 0 & 1\end{bmatrix}. \tag{20}$$

For the case with the beams pointing to $-4/M$, 0, and $4/M$, we have

$$\boldsymbol{F}=\begin{bmatrix}1 & \mathrm{e}^{\zeta\left(\sin\theta^2-\sin\theta^1\right)} & \mathrm{e}^{\zeta\left(\sin\theta^3-\sin\theta^1\right)}\\ \mathrm{e}^{\zeta\left(\sin\theta^1-\sin\theta^2\right)} & 1 & \mathrm{e}^{\zeta\left(\sin\theta^3-\sin\theta^2\right)}\\ \mathrm{e}^{\zeta\left(\sin\theta^1-\sin\theta^3\right)} & \mathrm{e}^{\zeta\left(\sin\theta^2-\sin\theta^3\right)} & 1\end{bmatrix}=\begin{bmatrix}1 & 0 & 0\\ 0 & 1 & 0\\ 0 & 0 & 1\end{bmatrix} \tag{21}$$

where $\zeta=\mathrm{j}\pi dM/\lambda$. For (20) and (21), we use $d=\lambda/2$ and the approximation with very small error, i.e., $\sin\theta\approx\theta$. Thus, we have $\boldsymbol{T}_2^{\mathrm{H}}\boldsymbol{T}_2=\boldsymbol{T}_1^{\mathrm{H}}\boldsymbol{T}_1$, so $\boldsymbol{T}_{\mathrm{sd}}$ is a unitary matrix and $\boldsymbol{n}_{\mathrm{Bsd}}$ is still Gaussian white noise vector, which is consistent with the basic assumption of ML estimation [31]. Next, substituting $\boldsymbol{T}_{\mathrm{sd}}$ for $\boldsymbol{T}$, and $\boldsymbol{B}_{\mathrm{sd}}$ for $\boldsymbol{B}$ in (7), we get

$$\underset{\theta_1,\theta_2}{\text{Maximize}}\ \sum_{l=1}^{L}\boldsymbol{x}_{\mathrm{Bsd}}^{\mathrm{H}}(l)\,\boldsymbol{P}_{\mathrm{Bsd}}(\theta_1,\theta_2)\,\boldsymbol{x}_{\mathrm{Bsd}}(l) \tag{22}$$

where $\boldsymbol{P}_{\mathrm{Bsd}}(\theta_1,\theta_2)=\boldsymbol{B}_{\mathrm{sd}}\left[\boldsymbol{B}_{\mathrm{sd}}^{\mathrm{H}}\boldsymbol{B}_{\mathrm{sd}}\right]^{-1}\boldsymbol{B}_{\mathrm{sd}}^{\mathrm{H}}$.

In addition, from the multipath geometry in Fig. 1, $\theta_2$ can be easily obtained [32] by the approximation with negligible error

$$\theta_2=f(\theta_1)\approx-\arcsin\left(\sin\theta_1+2h_{\mathrm{r}}/R_{\mathrm{d}}\right), \tag{23}$$

and we have $\boldsymbol{B}_{\mathrm{sd}}=\boldsymbol{T}_{\mathrm{sd}}^{\mathrm{H}}\boldsymbol{A}_I=\boldsymbol{T}_{\mathrm{sd}}^{\mathrm{H}}\left[\boldsymbol{a}(\theta_1)\ \boldsymbol{a}(f(\theta_1))\right]$. Thus, we only need to estimate the 1D parameter of $\theta_1$, and $\theta_2$ can be obtained from (23). The ML function can be rewritten as

$$\underset{\theta_1}{\text{Maximize}}\ \sum_{l=1}^{L}\boldsymbol{x}_{\mathrm{Bsd}}^{\mathrm{H}}(l)\,\boldsymbol{P}_{\mathrm{Bsd}}(\theta_1,f(\theta_1))\,\boldsymbol{x}_{\mathrm{Bsd}}(l). \tag{24}$$

With reference to [3,33], when the number of elements or SNR is large enough, the theoretical target elevation angle RMSE of the ML-SDB algorithm can be deduced to

$$\boldsymbol{E}_{\mathrm{SDBDML}}(\hat{\theta}_1)\approx\sqrt{\frac{M\sigma_n^2}{2}\mathrm{Re}^{-1}\left\{\boldsymbol{S}_P^{\mathrm{H}}\boldsymbol{D}^{\mathrm{H}}\boldsymbol{P}_{\mathrm{Bsd}}^{\perp}\boldsymbol{D}\boldsymbol{S}_P\right\}} \tag{25}$$

where $\mathrm{Re}\{\cdot\}$ denotes the real part, $\boldsymbol{S}_P=\sum_{l=1}^{L}\boldsymbol{c}(l)$, $\boldsymbol{D}=\boldsymbol{T}_{\mathrm{sd}}^{\mathrm{H}}\dfrac{\partial}{\partial\theta_1}\boldsymbol{A}_I$, and $P_{\mathrm{Bsd}}^{\perp}=\boldsymbol{I}-\boldsymbol{P}_{\mathrm{Bsd}}(\theta_1,f(\theta_1))$.

According to the idea of information theory, the ML-SDB algorithm has higher estimation accuracy than the 3D-BML algorithm, because the beamformer of the ML-SDB algorithm has wider spatial coverage and higher effective gain and uses geometry information. In addition, $h_{\mathrm{r}}\ll R_{\mathrm{d}}$, so neither antenna height error nor target distance error will affect the estimation accuracy of the ML-SDB algorithm.

### 3.3 RML-SDB algorithm

In this subsection, we take the refined signal model [3,25] into account in the ML-SDB algorithm. Utilizing the prior knowledge of surface reflection coefficient, and using a composite guide vector instead of a conventional guide vector, $\boldsymbol{B}_{\mathrm{sd}}$ can be replaced by

$$\begin{aligned}\boldsymbol{b}_{\mathrm{sd}}&=\boldsymbol{B}_{\mathrm{sd}}\begin{bmatrix}1\\ \rho\mathrm{e}^{-\mathrm{j}\varphi(\theta_1)}\end{bmatrix}=\\ &\boldsymbol{T}_{\mathrm{sd}}^{\mathrm{H}}\begin{bmatrix}\boldsymbol{a}(\theta_1) & \boldsymbol{a}(f(\theta_1))\end{bmatrix}\begin{bmatrix}1\\ \rho\mathrm{e}^{-\mathrm{j}\varphi(\theta_1)}\end{bmatrix}=\\ &\boldsymbol{T}_{\mathrm{sd}}^{\mathrm{H}}\left[\boldsymbol{a}(\theta_1)+\rho\mathrm{e}^{-\mathrm{j}\varphi(\theta_1)}\boldsymbol{a}(f(\theta_1))\right].\end{aligned} \tag{26}$$

Substituting $\boldsymbol{b}_{\mathrm{sd}}$ for $\boldsymbol{B}_{\mathrm{sd}}$ in (24), we get

$$\underset{\theta_1}{\text{Maximize}}\ \boldsymbol{F}(\theta_1)$$

where

$$\begin{aligned}\boldsymbol{F}(\theta_1)&=\sum_{l=1}^{L}\boldsymbol{x}_{\mathrm{Bsd}}^{\mathrm{H}}(l)\,\boldsymbol{P}_{\mathrm{bsd}}(\theta_1)\,\boldsymbol{x}_{\mathrm{Bsd}}(l)=\\ &\sum_{l=1}^{L}\boldsymbol{x}_{\mathrm{Bsd}}^{\mathrm{H}}(l)\,\boldsymbol{b}_{\mathrm{sd}}\left[\boldsymbol{b}_{\mathrm{sd}}^{\mathrm{H}}\boldsymbol{b}_{\mathrm{sd}}\right]^{-1}\boldsymbol{b}_{\mathrm{sd}}^{\mathrm{H}}\boldsymbol{x}_{\mathrm{Bsd}}(l)=\\ &\sum_{l=1}^{L}\frac{\boldsymbol{x}_{\mathrm{Bsd}}^{\mathrm{H}}(l)\,\boldsymbol{b}_{\mathrm{sd}}\boldsymbol{b}_{\mathrm{sd}}^{\mathrm{H}}\boldsymbol{x}_{\mathrm{Bsd}}(l)}{\boldsymbol{b}_{\mathrm{sd}}^{\mathrm{H}}\boldsymbol{b}_{\mathrm{sd}}}.\end{aligned} \tag{27}$$

The ML function can be simplified to

$$\underset{\theta_1}{\text{Maximize}}\ \sum_{l=1}^{L}\left|\frac{\boldsymbol{b}_{\mathrm{sd}}^{\mathrm{H}}\boldsymbol{x}_{\mathrm{Bsd}}(l)}{\sqrt{\boldsymbol{b}_{\mathrm{sd}}^{\mathrm{H}}\boldsymbol{b}_{\mathrm{sd}}}}\right|.$$

With reference to [3,33], when the number of elements or SNR is large enough, the theoretical target elevation angle RMSE of the RML-SDB algorithm can be deduced to

$$\boldsymbol{E}_{\mathrm{SDBDRML}}(\hat{\theta}_1)=\sqrt{\frac{M\sigma_n^2}{2\left|S_{p1}\right|^2}\left(\boldsymbol{D}_1{}^{\mathrm{H}}\boldsymbol{P}_{\mathrm{bsd}}^{\perp}\boldsymbol{D}_1\right)^{-1}} \tag{28}$$

where $S_{p1}=\sum_{l=1}^{L}\alpha(l)$, $\boldsymbol{P}_{\mathrm{bsd}}^{\perp}=\boldsymbol{I}-\boldsymbol{P}_{\mathrm{bsd}}(\theta_1)$, and $\boldsymbol{D}_1=\boldsymbol{T}_{\mathrm{sd}}^{\mathrm{H}}\dfrac{\partial\boldsymbol{b}_{\mathrm{sd}}}{\partial\theta_1}$.

Because the RML-SDB algorithm uses the prior knowledge of surface reflection coefficient and reduces the signal dimension, the RML-SDB algorithm has higher estimation accuracy and lower computational burden. However, the RML-SDB algorithm relies heavily on surface reflection conditions, i.e., its estimation perfor-

mance will severely reduce due to signal model mismatch [26] when the surface reflection parameters are unknown. On the contrary, the ML-SDB algorithm does not use the surface reflection parameters, i.e., it is not affected by the corresponding errors.

## 4. Computational complexity analysis

In this section, the computational complexity of the proposed algorithms, the MUSIC based on covariance matrix reconstructed (MUSIC-CMR) algorithm in [22], the 2D-BML and 3D-BML algorithms in [2] are analyzed.

Let the number of spatial search grid be $P$. The computational complexity of the MUSIC-CMR algorithm is $O(Q^2L+Q^3+QM+(M-U)^3+P(M-U)^2)$, where $U$ is the number of subarrays. The computational complexity of the 3D-BML and 2D-BML algorithms is $O(Q^2L+Q^3+QM)$. The RML-SDB and ML-SDB algorithms mainly considers the transformation from element-space to beamspace and the computation of objective function. The computational complexity of the transformation from element-space to beamspace is $O(QM)$. The computational complexity of the objective function of the two algorithms is $O(PQL)$ and $O(PQ^2L+Q^3)$. The computational complexity of these algorithms is summarized in Table 1. The order of algorithms in Table 1 is from small to large according to the computational complexity.

**Table 1 Computational complexity**

| Algorithm | Computational complexity |
|---|---|
| 2D-BML | $O(Q^2L+Q^3+QM)$ |
| 3D-BML | $O(Q^2L+Q^3+QM)$ |
| RML-SDB | $O(PQL+QM)$ |
| ML-SDB | $O(PQ^2L+Q^3+QM)$ |
| MUSIC-CMR | $O(Q^2L+Q^3+QM+(M-U)^3+P(M-U)^2)$ |

## 5. Simulation and real data processing results

In this section, the elevation estimation performance of the algorithms mentioned in Section 4 in multipath environment is discussed through several simulation scenarios and real data. The beams pointing for proposed algorithms are set to $-2/M$ and $2/M$. In MUSIC-CMR algorithm, the number of beams and subarrays are set to 5 and 15.

### 5.1 Simulations

Consider a digital array radar equipped with a uniform linear array with 30 elements where the distance between two adjacent array elements is $d=0.5$ m. We set $\lambda=1$ m, $h_r=8$ m, $R_d=20$ km, and $\rho=0.9\exp(\mathrm{j}\pi)$. For all simulations, the number of Monte Carlo trials is set to 500. These experiments are all performed on a PC with an Intel i7-7700 at 3.60 GHz and 8 GB of RAM. Let the SNR be defined as

$$\mathrm{SNR}=|\alpha|^2/\sigma_n^2 \tag{29}$$

Initially, we demonstrate the experimental and the theoretical target elevation angle RMSE of proposed algorithms against SNR. Assume that the radar receives only a single snapshot, and the target elevation angle is 4.5°. Fig. 5 illustrates the target elevation angle RMSE of proposed algorithms against SNR. Fig. 5 shows that the estimation error decreases with the increase of SNR. The experimental error is consistent with the theoretical error in high SNR, but the experimental error is higher than the theoretical error in low SNR because of approximation error. The RML-SDB algorithm performs better than the ML-SDB algorithm because of using the prior knowledge of surface reflection coefficient.

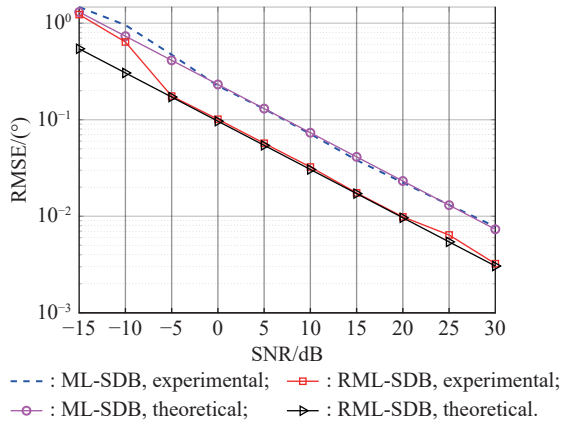


**Fig. 5 Theoretical and experimental RMSE of angle estimation against SNR**

The subsequent trials involve target elevation angle RMSE comparison of the algorithms mentioned in Section 4. For SNR = 10 dB, the target elevation angle RMSE of the five algorithms against angle are shown in Fig. 6 and Fig. 7, for 64 snapshots and a single snapshot, respectively. These figures show that the MUSIC-CMR algorithm is greatly affected by the number of snapshots, and the 2D-BML algorithm is not suitable for elevation estimation in multipath environment. The 3D-BML algorithm performs better than the previous two algorithms, but the performance is poor in high elevation area because of the insufficient spatial coverage. In addition, the RMSE of the 3D-BML algorithm is larger when the angle is 3.5°, which is caused by the phase of $\rho e^{-\mathrm{j}\varphi(\theta_1)}$ [2]. According to the simulation parameters, the phase of $\rho$ is $\pi$, and $\varphi(\theta_1)\approx 4\pi h_r\sin\theta_1/\lambda\approx 2\pi$, so the phase of $\rho e^{-j\varphi(\theta_1)}$

is $-\pi$, which results in the failure of the 3D-BML algorithm. The proposed algorithms perform better than other three algorithms, especially in high elevation area, because the beams setting of the proposed algorithms have better spatial coverage, which is consistent with Fig. 3. The RMSE of most algorithms is larger when the angle is small. The reason of this phenomenon is that the phase-difference between of direct and reflected signals gets closer to 180°, resulting in the mutual cancellation of the two signals. Fig. 8 illustrates the normalized power of ideal signal in element-space in multipath environment against angle. Fig. 8 shows that the signal power in low elevation area is obviously lower. In Fig. 6 and Fig. 7, the RMSE of the 2D-BML algorithm in low elevation area is not larger than the RMSE in high elevation area. That is because the beam directions of 2D-BML algorithm are 0 and $2/M$, which has a much higher gain for the direct signal than for the reflected signal and avoids the cancellation of the two signals.

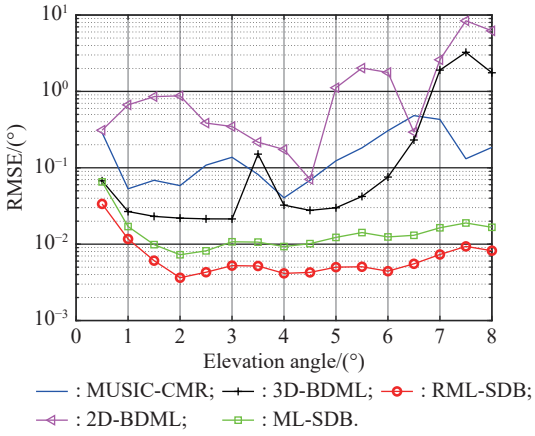


**Fig. 6 RMSE of angle estimation against angle for 64 snapshots**

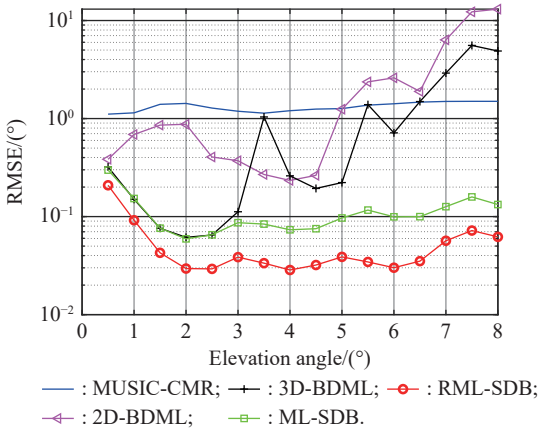


**Fig. 7 RMSE of angle estimation against angle for a single snapshot**

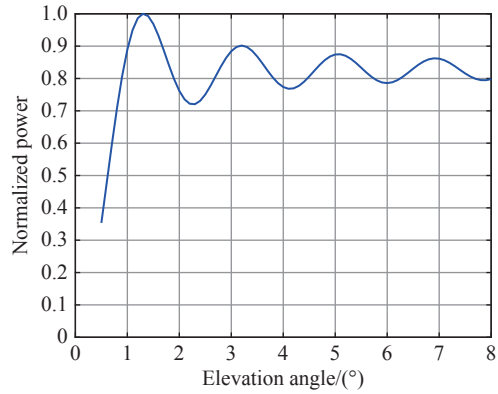


**Fig. 8 Normalized power of ideal signal in element-space in multipath environment against angle**

Thirdly, we show the target elevation angle RMSE of the ML-SDB algorithm with different beams setting against angle. For SNR = 10 dB, Fig. 9 illustrates the RMSE of the ML-SDB algorithm with different beams setting against angle. Specifically, the beam directions represented by the four lines in Fig. 9 are given in Table 2, and are denoted by 1D, 2D, 3D, and 3D2, respectively. Fig. 9 shows that the performance of the 1D algorithm is poor because of its insufficient beam degree of freedom and spatial coverage. The performance of the 2D algorithm and 3D algorithm is basically the same, which shows that simply increasing the number of beams is limited to improve the performance. The 3D2 algorithm performs better than other three algorithms in high elevation area, because the beams setting has wider spatial coverage, which is consistent with Fig. 4. In addition, the performance of 3D2 algorithm in low elevation area is not the best, because the beams setting is relatively scattered, which leads to the decrease of the effective gain in this area.

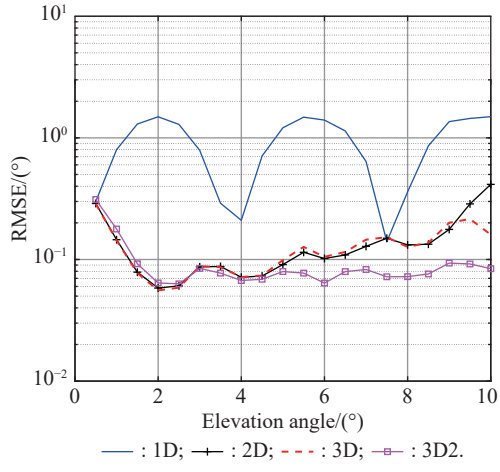


**Fig. 9 RMSE of target elevation angle with different beams setting against angle**

**Table 2 Meaning of the four lines in Fig. 9**

| Line type | Natation | Beam direction |
|---|---|---|
| Solid | 1D | 0 |
| Plus | 2D | $-2/M$, $2/M$ |
| Dotted | 3D | $-2/M$, 0, $2/M$ |
| Square | 3D2 | $-4/M$, 0, $4/M$ |

Finally, we analyze the influence of the errors of key parameters on the performance of the RML-SDB algorithm. Assuming that the SNR is 10 dB and the target elevation angle is 4.5°, the target elevation angle RMSE of the RML-SDB algorithm against the errors of antenna height, the amplitude and phase of reflection coefficient are shown in Fig. 10–Fig. 12, respectively. It is shown that the errors of antenna height and phase of reflection coefficient have a significant influence on the performance of the RML-SDB algorithm, while the amplitude error of reflection coefficient has a minor effect on the performance of the algorithm.

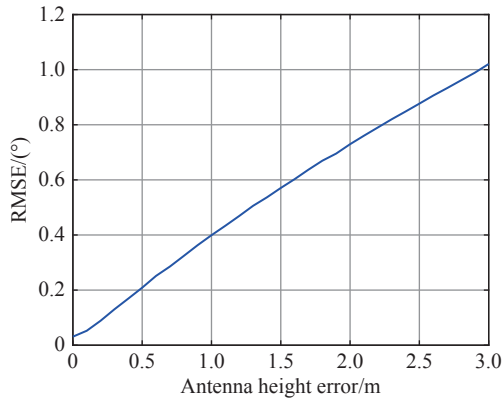


**Fig. 10 RMSE of target elevation angle against antenna height error**

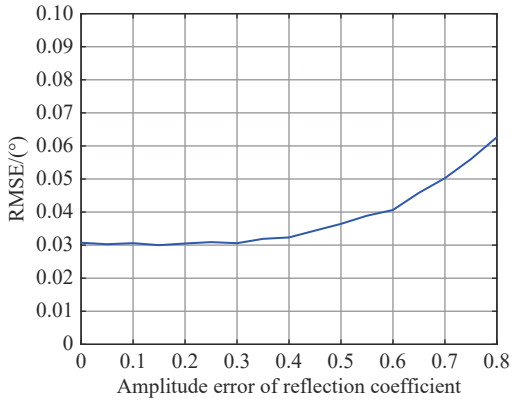


**Fig. 11 RMSE of target elevation angle against amplitude error of reflection coefficient**

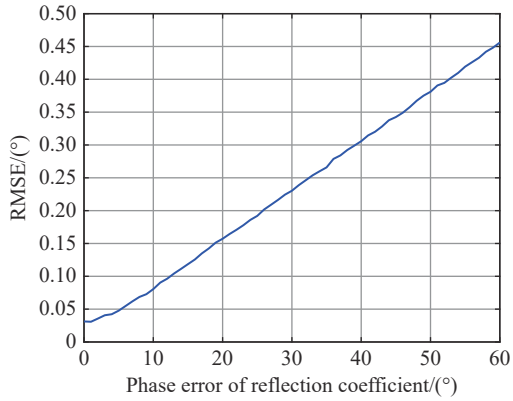


**Fig. 12 RMSE of target elevation angle against phase error of reflection coefficient**

## 5.2 Real data

The real data is applied to further verify the performance of the proposed algorithms. The radar works in the meter wave band and receives only a single snapshot. The terrain scenario is hilly, and the target is an airplane. Fig. 13 and Fig. 14 show the processed results of the real data by using the algorithms mentioned in Section 4. The processed results of the real data are displayed by height estimation results, which is even more interested in the engineering. The formula for calculating the height from the elevation angle is

$$h_t = h_r + R_d \sin(\theta_1) + R_d^2/(2R_e) \tag{30}$$

where $R_e$ is the effective radius of the Earth. The target height varies from 6 km to 10 km. It can be seen that the MUSIC-CMR algorithm is not suitable for this scene. The estimations of the 2D-BML and 3D-BML algorithms are less than the true elevation except for individual frames, because the spatial coverage of these two algorithms is insufficient in high elevation area. In addition, there are some singularities in the estimations of the 3D-BML algorithm, which shows that the 3D-BML algorithm is not very robust. The proposed algorithms perform better than other three algorithms. There are also some singularities in the estimations of the ML-SDB algorithm, but the overall situation is good. The RML-SDB algorithm obtains the optimal estimation without singularity.

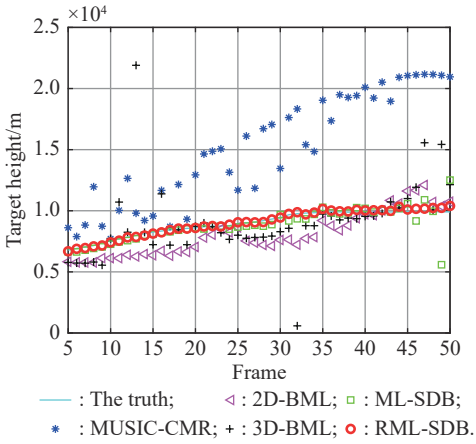


**Fig. 13 Estimation of target height against frames**

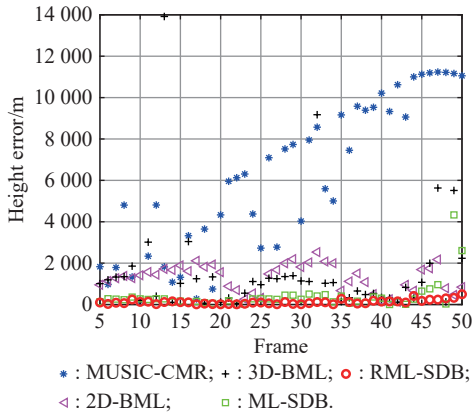


**Fig. 14 Estimation error of target height against frames**

## 6. Conclusions

In this paper, the problem of beamspace elevation estimation in multipath environment is discussed. Two beamspace ML algorithms based on sum and difference beams are proposed. The ML-SDB algorithm has higher estimation accuracy than the 3D-BML algorithm because of using the difference beams and geometry information, although the computational burden is higher. Compared with the ML-SDB algorithm, the RML-SDB algorithm has higher estimation accuracy and lower computational burden because of using the prior knowledge of surface reflection coefficient and reducing the signal dimension. However, the RML-SDB algorithm relies heavily on surface reflection conditions, i.e., its estimation performance will severely reduce when the surface reflection parameters are unknown. In addition, this paper analyzes two beam settings for proposed algorithms, which can be adjusted according to actual needs. Generally speaking, the two beam pointing conditions of $\boldsymbol{T}_{\mathrm{sd}}$ in Fig. 3 and Fig. 4 meet the needs of most low elevation estimation scenarios, where the elevation range is below 12°.

Additionally, multiple targets can generally be separated in the range, Doppler, and angle dimensions by signal processing. If there are multiple targets in the same range unit, Doppler channel, and beam direction, the proposed method will fall due to signal model mismatch.

## References

[1] BARTON D K. Low-angle radar tracking. Proc. of the IEEE, 1974, 62: 687–704.
[2] ZOLTOWSKI M D, LEE T S. Beamspace ML bearing estimation incorporating low-angle geometry. IEEE Trans. on Aerospace and Electronic Systems, 1991, 27: 441–458.
[3] ZHU Y T, ZHAO Y B, SHUI P L. Low-angle target tracking using frequency-agile refined maximum likelihood algorithm. IET Radar, Sonar & Navigation, 2016, 11(3): 491−497.
[4] LIU Y, LIU H, XIA X G, et al. Projection techniques for altitude estimation over complex multipath condition-based VHF radar. IEEE Journal of Selected Topics in Applied Earth Observations and Remote Sensing, 2018, 11(7): 2362−2375.
[5] MAHAFZA R B. Radar systems analysis and design using matlab. 3rd ed. New York: CRC Press, 2013.
[6] KERR D E. Propagation of short radio waves. 2nd ed. London: Peter Perrgrinus Ltd., 1987.
[7] SKOLNIK I. Radar handbook. 3rd ed. New York: The McGraw-Hill Companies, 2008.
[8] HAN S F, I C L, XU Z, et al. Large-scale antenna systems with hybrid analog and digital beamforming for millimeter wave 5G. IEEE Communications Magazine, 2015, 53(1): 186−194.
[9] ZHAO Y B, PANG X J, CHEN S J. A reduced-dimension RML method for transmit beamspace-based MIMO radar. Digital Signal Processing, 2021, 114: 103072.
[10] ZOLTOWSKI M D, KAUTZ G M, SILVERSTEIN S D. Beamspace root-MUSIC. IEEE Trans. on Signal Processing, 1993, 41(1): 344–364.
[11] GAO X Y, DAI L L, HAN S F. Reliable beamspace channel estimation for millimeter-wave massive MIMO systems with lens antenna array. IEEE Trans. on Wireless Communications, 2017, 16(9): 6010–6021.
[12] BUCHANAN K, ROCKWAY J, STERNBERG O. Sum-difference beamforming for radar applications using circularly tapered random arrays. Proc. of the IEEE Radar Conference, 2016. DOI: 10.1109/RADAR.2016.7485289.
[13] IWAZAKI S, ICHIGE K. Sum and difference composite co-array: an extended array configuration toward higher degree of freedom. Proc. of the International Conference on Advances in Electrical, Electronic and Systems Engineering, 2016: 333−338.
[14] ZHU L, QIU S, HAN Y B. Combined constrained adaptive sum and difference beamforming in monopulse angle estimation. IEEE Antennas and Wireless Propagation Letters, 2018, 17(12): 2314–2318.
[15] ZHAO J Y, WANG Y L, LI R F, et al. Adaptive monopulse angle measurement for meter-wave radar based on differential constraints technique. Proc. of the IEEE 11th International Conference on Signal Processing, 2012. DOI: 10.1109/ICoSP.2012.6491918.
[16] HE Y D, ZHOU J, ZHOU B H. Adaptive sum and difference beamforming for monopulse system with array antennas. Proc. of the 6th International Conference on Wireless Com-

munications Networking and Mobile Computing, 2010. DOI: 10.1109/WICOM.2010.5600714.
[17] XU Z H, XIONG Z Y, WU J N. Symmetrical difference pattern monopulse for low-angle tracking with array radar. IEEE Trans. on Aerospace & Electronic Systems, 2017, 52(6): 2676–2684.
[18] ZHUO J, SUN C. Experimental studies on the multistage constant modulus array for the estimation of directions-of-arrival. Chinese Journal of Acoustics, 2004(3): 268−277.
[19] YIN D Y, ZHANG F. Uniform linear array MIMO radar unitary root MUSIC angle estimation. Proc. of the Chinese Automation Congress, 2020: 578−581.
[20] LI S E, ZHANG Y, EDWARDS R. Two dimension DOA ESPRIT algorithm based on parallel coprime arrays and complementary sequence in MIMO communication system. Proc. of the IEEE International Conference on Signal, Information and Data Processing, 2019. DOI: 10.1109/ICSIDP47821.2019.9173170.
[21] PAN J J, SUN M, WANG Y D. An enhanced spatial smoothing technique with ESPRIT algorithm for direction of arrival estimation in coherent scenarios. IEEE Trans. on Signal Processing, 2020, 68: 3635–3643.
[22] YANG R T, GRAY D, AL-ASHWAL W. Estimation of the DOAs of coherent signals in beam space processing for phased arrays. Proc. of the International Conference on Radar, 2018. DOI: 10.1109/RADAR.2018.8557250.
[23] LIU Y, HOU L N, SHEN Q M. Beamspace U-ESPRIT DOA estimation algorithm of coherently distributed sources in massive MIMO systems. Proc. of the 12th International Conference on Advanced Computational Intelligence, 2020: 126−132.
[24] ZISKIND I, WAX M. Maximum likelihood localization of multiple sources by alternating projection. IEEE Trans. on Acoustics, Speech, and Signal Processing, 1988, 36(10): 1553–1560.
[25] LO T, LITVA J. Use of a highly deterministic multipath signal model in low-angle tracking. IEE Proceedings F-Radar Signal Processing, 1991, 138: 163–171.
[26] WANG S H, CAO Y H, SU H T, et al. Target and reflecting surface height joint estimation in low-angle radar. IET Radar Sonar Navigation, 2016, 10(3): 617–623.
[27] KIM J, YANG H J, KWAK N. Low-angle tracking of two objects in a three-dimensional beamspace domain. IET Radar Sonar & Navigation, 2012, 6(1): 9–20.
[28] LIU J, LIU Z, XIE R. Low angle estimation in MIMO radar. Electronics Letters, 2010, 46(23): 1565–1566.
[29] XU B Q, ZHAO Y B. Transmit beamspace-based DOD and DOA estimation method for bistatic MIMO radar. Signal Processing, 2019, 157: 88–96.
[30] JAO J K. A matched array beamforming technique for low angle radar tracking in multipath. Proc. of the IEEE National Radar Conference: 1994, 171–176.
[31] BOMAN K, STOICA P. Low angle estimation: models, methods, and bounds. Digital Signal Processing, 2001, 11(1): 35–79.
[32] CHEN S, ZHAO Y B, HU Y L, et al. A beamspace maximum likelihood algorithm for target height estimation for a bistatic MIMO radar. Digital Signal Processing, 2022, 122: 103330.
[33] STOICA P, NEHORAI A. MUSIC, maximum likelihood, and Cramer-Rao bound: further results and comparisons. Proc. of the International Conference on Acoustics, Speech, and Signal Processing, 1989: 2605−2608.

## Biographies

**CHEN Sheng** was born in 1993. He received his B.S. degree from Xidian University, Xi'an, China, in 2017. He is pursuing his Ph.D. with Department of Electrical Engineering, Xidian University. His research interests include array signal processing and low-angle estimation with digital array radar.
E-mail: 842561535@qq.com

**ZHAO Yongbo** was born in 1972. He received his M.E. and Ph.D. degrees in electrical engineering from Xidian University, Xi'an, China, in 1997 and 2000, respectively. He is a professor with the National Laboratory of Radar Signal Processing, Xidian University. His research interests include adaptive signal processing, array signal processing, multiple input multiple output (MIMO) radars, and target tracking.
E-mail: ybzhao@xidian.edu.cn

**HU Yili** was born in 1994. He received his B.S. degree in signal and information processing from Yangtze University, JingZhou, China, in 2017. He is working toward his Ph.D. degree in the National Laboratory of Radar Signal Processing, Xidian University. His research interests include processing of airborne conformal arrays radar, clutter suppression and multiple input multiple output (MIMO) radar signal processing.
E-mail: huyili66@126.com

**PANG Xiaojiao** was born in 1993. She received her B.S. degree from Xidian University, Xi'an, China, in 2016. She is pursuing her Ph.D. degree with Department of Electrical Engineering, Xidian University. Her research interests are space time adaptive processing and compress scene.
E-mail: 1964230291@qq.com